JCTC Journal of Chemical Theory and Computation

Implicit Solvent Models and the Energy Landscape for Aggregation of the Amyloidogenic KFFE Peptide

Birgit Strodel and David J. Wales*

University Chemical Laboratories, Lensfield Road, Cambridge CB2 1EW, U.K.

Received November 9, 2007

Abstract: This study compares the performance of four implicit solvent models in describing peptide aggregation. The solvent models are the effective energy function-1 (EEF1) and three generalized Born (GB) models: one following the original implementation of Still (GB1), the analytical continuum electrostatics (ACE) potential, and GB with "simple switching" (GBSW). For each solvent model the first step of aggregation, namely dimerization, is investigated for the KFFE peptide, which is one of the shortest peptides known to form amyloid fibrils in vitro. Using basin-hopping for global optimization and replica exchange molecular dynamics simulations, we conclude that of the four solvent models considered, the EEF1 potential provides the most reliable description for the formation of KFFE amyloid precursors. It produces results that are closest to the experimental findings of a partial β-strand conformation for the KFFE peptide in solution along with the formation of fibrils exhibiting antiparallel β-strand structure. The ACE and GB1 potentials also show a significant β-propensity for the KFFE peptide but fail to produce stable KFFE dimers. The GBSW potential, on the other hand, supports a very stable antiparallel dimer structure, but in a turn rather than a β conformation.

1. Introduction

Implicit solvent models are based on the assumption that ensemble averages of interactions between the solute and explicit solvent molecules can be approximated by a mean field formalism, which is expressed as a function of the solute configuration alone. Explicit solvent molecules can then be omitted, thereby reducing the computational cost due to the reduced system size and the absence of solvent relaxation. Several approaches exist to describe the solute−solvent interactions by their mean field behavior. In many of these models the solvation free energy, ΔG_{solv}, is decomposed into electrostatic (el) and nonpolar (np) contributions, $\Delta G_{solv} = \Delta G_{el} + \Delta G_{np}$. The nonpolar contribution to ΔG_{np} includes the energetic penalty for forming a cavity in the solvent and the solute−solvent van der Waals (vdW) dispersion interactions.[1] In most implicit solvent models ΔG_{np} is treated entirely empirically by approximating it as product of the solvent-exposed surface area of the solute and a phenomenological surface tension coefficient. For the calculation of the electrostatic contribution the solvent is treated as a homogeneous, high-dielectric medium, which surrounds the cavity containing the low-dielectric solute with explicit charges at the atomic centers. The Poisson–Boltzmann (PB) equation provides a rigorous formulation for the calculation of ΔG_{el} and can be solved numerically for the electrostatic potential throughout space. However, the cost involved in obtaining accurate PB results and the difficulties in obtaining continuous first derivatives have limited the application of PB theory in biomolecular simulations; in most applications, the method is used as a benchmark for other implicit solvent models.

An alternative approach is provided by the generalized Born (GB) formalism, which is based on the same continuum electrostatic model for the solvent as the PB theory, but is computationally more efficient and can reproduce the PB results accurately. The starting point is the Born formula,

$$\Delta G_{el} = -\frac{\tau q^2}{2R} \quad \text{with} \quad \tau = \frac{1}{\epsilon_p} - \frac{1}{\epsilon_s} \tag{1}$$

which is the analytical solution of the PB equation for a single charge q in a sphere of radius R with (low) dielectric constant ϵ_p, embedded in a solvent with (high) dielectric

* Corresponding author. E-mail: dw34@cam.ac.uk.

10.1021/ct700305w CCC: $40.75
Published on Web 03/14/2008

constant ϵ_s. In the GB model, this formula is generalized for a polyatomic system occupying a more complex shape. One of the most reliable and widely used GB formulations is that of Still et al.,[2]

$$\Delta G_{el} = -\frac{\tau}{2}\sum_{i,j}\frac{q_i q_j}{\sqrt{r_{ij}^2 + R_i^{GB}R_j^{GB}\exp(-r_{ij}^2/4R_i^{GB}R_j^{GB})}} \quad (2)$$

where r_{ij} is the distance between atoms i and j, q_i and q_j are their respective charges, and R_i^{GB} denotes the effective Born radius. The Born radius can be understood as the distance from an atom to the dielectric boundary, and successful application of the GB model depends upon an appropriate evaluation of this quantity. In most GB methods the so-called Coulomb field approximation (CFA) is invoked, which is exact for a charge in the center of a spherical cavity and assumes that the dielectric displacement is Coulombic in form and remains so even when the external dielectric is altered in the solvation process. The CFA allows us to calculate the self-electrostatic energy, $\Delta G_{el,i}$, of atom i, and comparison with the Born equation (1) results in

$$\frac{1}{R_i^{GB}} = -\frac{2\Delta G_{el,i}}{\tau q^2} = \frac{1}{R_i} - \frac{1}{4\pi}\int_{solute,r>R_i}\frac{1}{r^4}\,dV \quad (3)$$

where R_i is the atomic radius, e.g., vdW radius, used to define the solute cavity filling the volume V, over which the integral is calculated.

Most of the GB methods differ in how the volume integral in eq 3 is calculated. It can be approximated as a discrete sum of overlapping spheres[3–6] or Gaussians[7] or by carrying out the integration numerically, either by reformulating the volume integral into a surface integral,[8] using a cubic integration lattice,[9] or employing integration techniques adapted from density functional theory.[10] The success of a GB model in reproducing PB results depends on how the solvent boundary at the molecular surface is defined for the evaluation of the volume integral, and various improvements addressing this issue have been proposed in recent years.[5,11] Another limitation of GB models, which might lead to deviations from the PB result, is the CFA, which is not valid for charges in nonspherical cavities. In the latest GB models, empirical higher-order correction terms that extend eq 3 beyond the CFA have been suggested, and it was shown that this approach further improves the solvation energies.[6,10,12,13]

In this study, we investigate the performance of three different GB models, which are implemented in CHARMM.[14] Two of them, called GB1[15] and ACE,[7] use the pairwise summation of atomic volumes to approximate the volume integral (3), while the third, GBSW,[11] employs a direct evaluation of the molecular volume. Alternative implicit solvent models concentrate on the screening of electrostatic interactions in the solute due to solvation. One of these methods is the effective energy function EEF1, which is also implemented in CHARMM and modulates the screening as a function of the solvent-excluded volume. The EEF1 solvation model is also considered in the present contribution.

Implicit solvent models have been used successfully for a variety of applications, such as distinguishing native and near-native structures from nonnative decoys[16–21] and studying polypeptide folding and unfolding in atomic detail.[22–24] In recent years, there have also been a number of comparative studies of the various implicit solvent models aiming to identify their advantages and limitations for particular applications. The outcome of these studies is as different as the systems investigated and it seems that, at least for the moment, no single model performs best in all situations. Steinbach, for instance, found that EEF1 performed better than ACE and the surface-area model SASA[25] in identifying near-native states for the three peptides trp-cage, BS1 and U(1-17)T9D.[21] Stultz concluded that only the explicit solvent model TIP3P[26] was able to correctly predict the experimental end-to-end distance distribution for a twelve-residue peptide from rat tyrosine hydroxylase, while none of the implicit solvent models EEF1, ACE, GB1, and SASA were successful.[27] Huang and Stultz investigated whether the three implicit solvent models EEF1, GB1, and GBSW could reproduce the set of potential energy minima obtained from explicit solvent simulations with the TIP3P water model for the six-residue peptide PHF6.[28] They concluded that all three implicit solvent models were in good agreement with the results from explicit solvent simulations and that EEF1 provided the best representation of the most favored conformations. However, in an assessment of various implicit solvent models for the description of peptide−surface interactions, EEF1 performed badly and ACE was best when compared to results obtained from density functional theory combined with the self-consistent reaction field implicit solvent model.[29]

The objective of the present work is to compare the results for EEF1, ACE, GB1, and GBSW when applied to peptide aggregation. To this end, we consider the tetrapeptide KFFE, which is one of the shortest peptides known to form amyloid fibrils in vitro.[30] In this study, we focus on the first step in the aggregation process, namely dimerization. In a study by Baumketner and Shea,[31] this process was investigated using the GB1 solvent model and compared to experiment.[30] In other simulations the formation mechanism of larger KFFE oligomers, ranging from tetramers to heptamers, was analyzed in detail using a combination of all-atom molecular dynamics (MD) simulations in explicit solvent and the activation-relaxation technique coupled with a coarse-grained potential.[32–35] The focus of the current work, however, is not to investigate the mechanism of dimerization but rather to study the influence of the potentials on the conformations of the dimer. Implicit solvent models have already been used in simulations examining the process of oligomer formation of amyloidogenic peptides,[31,36–39] but we are not aware of any study that has checked whether implicit solvent models are capable of capturing the correct mechanistic details and oligomeric structures. Compared to investigations of the conformational equilibria of a single peptide, simulations of peptide oligomerization entail an additional layer of complexity. Not only do the solvation forces and intramolecular forces have to be represented correctly but intermolecular forces come into play. In this sense, the KFFE peptide is an

interesting test case, since it is short with opposite charges at the termini, leading to strong competition between Coulomb interactions within the peptide, between the peptides, and between the peptide and the solvent. In addition, the two middle residues of KFFE are aromatic and hydrophobic and, hence, probably promote the dimerization as a result of hydrophobic and $\pi-\pi$ interactions. Such competing forces all have to be accounted for in the potential and any imbalance is likely to be particularly noticeable for relatively short and highly charged peptides.

To assess the performance of the four implicit solvent models in question in describing the aggregation of KFFE, we used basin-hopping[40–43] (BH) global optimization and replica exchange molecular dynamics[44] (REMD) to explore the energy landscape of the KFFE monomer and dimer. In the next section, more details of the BH approach and REMD are provided, followed by the results, which vary significantly between the implicit solvent models. Our discussion focuses on the origin of these differences and points out possible opportunities for improvement. In Appendix A, we describe the solvent models, and in Appendix B, we outline the details of a REMD simulation using explicit TIP3P water,[26] which we have performed for comparison. In Appendix C, we discuss problems regarding the numerical convergence that we encountered during calculations with the GBSW implicit solvent model.

2. Methods

Experimentally,[30] the KFFE peptide has charged termini, NH_3^+-Lys-Phe-Phe-Glu-COO^-, and we performed simulations of the corresponding system using the CHARMM software (version c31a2).[14] Four implicit water models, EEF1,[45] ACE,[7] GB1,[15] and GBSW[11] were used in combination with three protein empirical potentials. The united-atom CHARMM19 parameters[46] were employed for the ACE and GB1 solvent models, a modified version of CHARMM19 was used with the EEF1 solvent model,[45] and the all-atom CHARMM22 potential[47] along with the CMAP modifications[48–50] was employed for the GBSW solvent model. These three choices will be referred to as C19, C19E, and C22, respectively. The four implicit solvent models are described in detail in Appendix A.

2.1. Basin-Hopping Global Optimization. The basin-hopping (BH) approach to global optimization[40–43] can be viewed as a generalization of the Monte Carlo plus energy minimization procedure of Li and Scheraga.[51] Moves are proposed by perturbing the current geometry and are accepted or rejected based upon the energy difference between the local minima obtained following minimization from the two instantaneous configurations. In effect, the potential energy surface is transformed into the basins of attraction[43,52,53] of all the local minima, so that the energy for configuration $\mathbf{r}$ is

$$\tilde{E}(\mathbf{r}) = \min\{E(\mathbf{r})\} \quad (4)$$

where min denotes minimization. Large steps can be taken to sample this transformed landscape, since the objective is to step between local minima. Furthermore, there is no need to maintain detailed balance when taking steps, because the BH approach attempts to locate the global potential energy minimum and is not intended to sample thermodynamic properties. Basin-hopping has already been employed to find the global minimum of peptides and proteins.[54–60] The moves for perturbing the current geometry of the KFFE peptides were taken in the dihedral angle space ϕ and ψ.[61] A number of these backbone dihedrals were selected and then twisted by a maximum angle, which was initially set to 30°. To select the dihedrals, we followed earlier work[61] and chose different twisting probabilities depending on the position along the peptide chain. The relative probabilities were highest for the two ends of the chain, lowest for the middle of the chain, and varied linearly between the ends and the middle. The probabilities for the ends and the middle of the chain were set to 0.4 and 0.2 for all BH runs.

Since one objective of this study was to find the global potential minimum for dimers, rigid body moves for whole peptide chains were implemented within the BH algorithm. The simplest of these moves were rigid body translation and rotation of one peptide chain, rotating around the local center of mass. Rigid body moves were performed every 10 or 20 BH steps. In most basin-hopping runs, the maximum values for translation and rotation were initially set to 1.0 Å and 60°, respectively. However, all move sizes for rigid-body and dihedral-angle moves were automatically adjusted every 50 steps during each BH run to produce an average acceptance ratio of 0.3. To further increase the efficiency of the BH algorithm for peptide oligomers, we also implemented a so-called internal rigid body move. The idea is to randomly select one of the four possible end-to-end vectors between the two peptide chains, rotate one of the peptides around it through a random angle, and rescale the end-to-end distance by a random factor within user defined limits. Because this type of move generally leads to a substantial change in geometry, it was only applied every 100 to 500 BH steps. Furthermore, it is very likely that after such an internal rigid body move the energy of the new local minimum will be much higher than that of the original minimum. If the energy exceeded a user defined value, the step was rejected and a fresh internal rigid body move was attempted until an acceptable move was found. For the resulting geometry small rigid body translation and rotation, as well as dihedral moves, were applied for a fixed number of steps between 100 and 200, without employing the acceptance criterion, to allow the dimer to relax. If a suitable minimum was found, the previous minimum was replaced with it; if it was not, the geometry was reset to the structure from which the internal rigid body move was initiated.

2.2. Replica Exchange Molecular Dynamics. We used replica exchange molecular dynamics (REMD),[44] as implemented in the MMTSB tool set,[62] to explore the conformational space of the KFFE dimer modeled with each of the CHARMM force fields and solvent models. In the REMD protocol multiple simulations of the same system (replicas) are run simultaneously at different temperatures. Every τ time steps an attempt is made to swap temperatures between two different replicas i and j. The exchanges are accepted with probability $\min\{1, \exp(-\Delta)\}$, where $\Delta = (1/k_B T_i - 1/k_B T_j)(E_j - E_i)$, and k_B is the Boltzmann constant, T_i and E_i denote

the temperature and potential energy of replica i, respectively, and j is typically replica $i + 1$ at the same time step. The temperatures for the replicas were exponentially spaced between a minimum value T_{min} and a maximum value T_{max}. This procedure allows for an improved sampling of the conformational space at low temperatures, since crossing potential energy barriers is facilitated at higher temperatures, and the resulting conformational changes migrate into the lower T replicas.[63] The dynamics were propagated using the Langevin method, with a time step of $\delta t = 1$ fs and a friction coefficient of $\zeta = 20$ ps^{-1}. The SHAKE algorithm[64,65] was used to freeze out bond vibrations involving hydrogen atoms. A time step of 1 fs combined with SHAKE guarantees stable trajectories for simulations with implicit solvent models.[66] The data collected during each REMD simulation were analyzed using the weighted histogram analysis method.[67]

For MD simulations of the KFFE dimer with implicit solvent, it was necessary to confine the peptides by repulsive walls to model constant concentration conditions and to prevent the peptides from drifting away. We used a spherical container, and the confining potential experienced by an atom located at $\mathbf{r}$ is then[68]

$$V_c(r) = \frac{4\pi eR}{5r}\left[\left(\frac{\sigma}{r-R}\right)^{10} - \left(\frac{\sigma}{r+R}\right)^{10}\right] \quad (5)$$

where $r = |\mathbf{r}|$ and $\mathbf{r} = \mathbf{0}$ is the center of the sphere with radius R. The parameters σ and e were chosen to be 1 Å and 1 kcal mol^{-1}, respectively.[31] The potential (5) guarantees short-range repulsive interactions between peptide atoms and the inner walls of the container. The container radius was chosen to be $R = 25$ Å, which corresponds to a molecular concentration of 50 mM. This concentration is about two orders of magnitude higher than the concentration that was used in the experiment by Tjernberg et al. to investigate the aggregation of KFFE.[30] In the current theoretical study, lower concentrations were not possible, because two of the implicit solvent models prevented the KFFE peptides from dimerizing when a container radius of $R = 43$ Å or more was used, which corresponds to a concentration of 10 mM or lower. This problem is discussed in more detail in section 3.2.

3. Results

3.1. KFFE Monomer. *Conformational Space of the Monomer.* Before analyzing the performance of the various potentials for the dimerization of the KFFE peptide, it is instructive to investigate their impact on the conformations of the KFFE monomer. We therefore started with a BH run for each of the four solvent models to locate the corresponding global potential minimum. In each case, it was sufficient to perform a single BH run consisting of 5000 steps at a temperature of 300 K. It is likely that the β-propensity of a peptide plays a crucial role in determining whether or not that peptide forms amyloid aggregates.[30,69] To investigate the β-propensity of the KFFE peptide, the C_α-rmsd from the β-strand illustrated in Figure 1A was calculated for each accepted local minimum during the BH run, and the structure lowest in potential energy with an rmsd < 0.5 Å was saved along with the global potential minimum. The EEF1, GB1, and GBSW potentials produce a type VIII β-turn[70] for the global potential minimum, which is shown in Figure 1B. This structure is stabilized by salt bridges between the oppositely charged N and C termini, as well as hydrogen bonds between these two residues. The comparison between strand and turn reveals that for the GBSW potential the β-strand is disfavored most, lying 12.2 kcal mol^{-1} above the turn structure, whereas for EEF1 and GB1 this difference is only 7.1 and 6.3 kcal mol^{-1}, respectively. The ACE potential has the β-strand as the global potential minimum, which is, however, only 0.7 kcal mol^{-1} lower in energy than a turn-like structure shown in Figure 1C.

To further explore the conformational space of the KFFE monomer, we performed REMD simulations with six replicas exponentially distributed between 250 and 450 K, giving a uniform acceptance ratio for exchanges with values between 0.35 and 0.45 for all REMD simulations. The simulations consisted of 100 000 replica exchange cycles, each involving 1000 MD time steps, resulting in a total simulation time of 100 ns for each potential. All replica runs were started from random structures, selected from a previous high temperature MD run. Before data were collected, 2000 MD steps were applied for equilibration. In the production phase, we saved the C_α-rmsd from the β-strand, rmsd$_\beta$, and the turn, rmsd$_t$. The resulting free energy surface (FES) is shown in Figure 1 for $T = 300$ K as a function of rmsd$_\beta$ and rmsd$_t$. The surfaces for the EEF1 and GB1 potentials are similar. Both are dominated by a broad minimum for strand-like structures, whereas the turn configuration plays a minor role. Instead, a structure intermediate between the strand and turn (Figure 1C) is the second-most populated structure for the monomer modeled by the EEF1 and GB1 potentials. For the ACE potential, the latter structure is the most pronounced free energy minimum, followed by the β-strand, whereas the turn is hardly populated. The FES for the KFFE peptide modeled by the GBSW potential is very distinct from the EEF1, GB1, and ACE surfaces. The only pronounced free energy minimum here is the turn motif, whereas the β-strand and the intermediate structure are $\gtrsim$4 kcal mol^{-1} higher in free energy.

The conclusion from the REMD results is that the EEF1, ACE, and GB1 potentials produce a considerable β-propensity for the KFFE peptide, in accord with experiment.[30] Comparison with the BH results reveals that the β-strand is favored by entropy and the turn is stabilized by potential energy. In the case of the GBSW potential, this stabilization is larger than the energy gain from the increased entropy for the β-strand, resulting in a very low β-propensity of the KFFE peptide.

Energy Analysis for the β-Strand and Turn. To understand the origin of the low β-propensity of the KFFE peptide modeled by the GBSW potential, we considered the total energy, E_{tot}, decomposed into the solvation free energy, ΔG_{solv}, and the vacuum potential energy, $V_{vac} = V_{bond} + V_{el} + V_{vdW}$. Here, V_{bond} represents all the bonded interactions, V_{vdW} is the van der Waals interaction treated by a 6−12 potential, and the electrostatic interactions V_{el} are modeled by a Coulomb potential of atom-centered point charges. These contributions are listed in Table 1 for the most stable β-strand and turn obtained for each potential. We note,

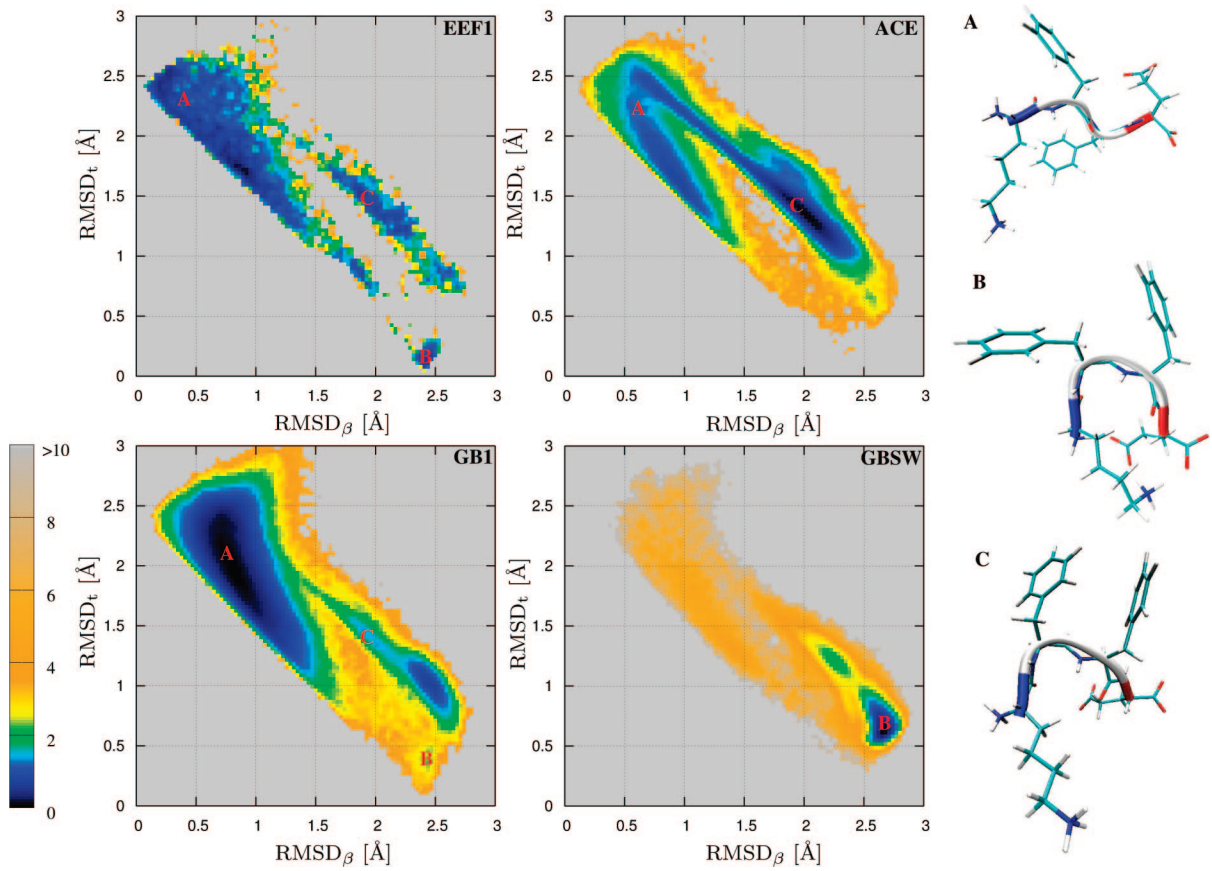

Figure 1. Free energy surfaces at $T = 300$ K in terms of the C_α-rmsd from the β-strand, rmsd$_\beta$, and from the turn, rmsd$_t$, for the KFFE monomer described by the implicit solvent models EEF1, ACE, GB1, and GBSW. The energy scale (in kilocalories per mole) is given on the left. The structures for the free energy minima are shown on the right, which are (A) a β-strand, (B) a turn, and (C) an intermediate structure between strand and turn.

Table 1. Total Energy, E_{tot}, Decomposed into the Solvation Free Energy, ΔG_{solv}, and Vacuum Energy, $V_{vac} = V_{bond} + V_{el} + V_{vdW}$ for the β-Strand and Turn of the KFFE Monomer[a]

solvent model	β-strand					turn				
	E_{tot}	ΔG_{solv}	V_{bond}	V_{el}	V_{vdW}	E_{tot}	ΔG_{solv}	V_{bond}	V_{el}	V_{vdW}
EEF1[b]	−156.1	−87.7 (56%)	7.1	−58.8	−16.6	−163.2	−80.3 (49%)	12.2	−75.2	−19.8
ACE	−475.1	−304.8 (64%)	5.0	−154.2	−21.1	−474.4	−208.9 (44%)	6.9	−250.9	−21.5
GB1	−483.1	−325.8 (67%)	6.2	−145.4	−18.2	−489.4	−193.4 (39%)	7.5	−277.4	−26.1
GBSW	−211.4	−302.7 (143%)	20.4	61.2	9.7	−223.6	−153.6 (69%)	18.6	−104.4	15.8

[a] All values are in kilocalories per mole. The values in parentheses are the percentage contribution of ΔG_{solv} to E_{tot}. [b] The electrostatic energies, V_{el}, are not really vacuum values for the EEF1 potential, because the C19E force field has charge screening incorporated into its parameters.

however, that for the EEF1 potential V_{el} is not the vacuum energy, since by design it contains the charge screening by the solvent. For each potential, the β-strand is favored by solvation and the turn by internal stabilization, but the relative values are different between the potentials. Most distinct is the GBSW potential, which produces a positive value of V_{vac} for the β-strand, and thus the stabilization of this structure entirely derives from ΔG_{solv}. We note that the vacuum potential energy, V_{vac}, is really a property of the underlying force field, i.e. C19E, C19, and C22, rather than the solvent model. Hence, the ACE and GB1 potentials, both used together with C19, give similar results for the energy contributions. For all three force fields, V_{bond} is always positive for both structures. For C19E and C19 the vdW interactions stabilize the β-strand and turn by about 20 kcal mol^{-1}, whereas for C22 both structures are disfavored in terms of vdW interactions. In each case, the electrostatic interactions provide the largest contribution to V_{vac} and stabilize the structures, except for the β-strand when modeled with C22. The Coulomb interactions are, however, diminished by the charge screening due the surrounding solvent, as the comparison between the values of V_{el} for the C19E and C19 force fields reveals. From these values, we estimate that the aqueous solvent reduces the Coulomb interactions by 90−100 kcal mol^{-1} in the β-strand, where the terminal charges are quite far apart. The salt bridges in the turn are screened substantially, reducing their stability by 180−200 kcal mol^{-1}.

To study the effect of solvent charge screening for each residue, we have decomposed V_{el} into its residue−residue contributions, as shown in Figure 2. As expected, the stabilization of the turn modeled by the C19 (ACE and GB1)

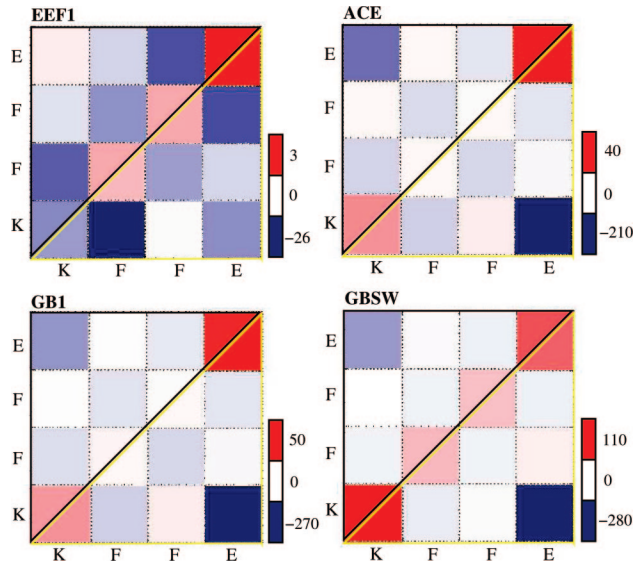

Figure 2. Residue–residue map of the electrostatic interaction energy, V_{el}, for the β-strand (upper triangle, black) and turn (lower triangle, yellow) conformations of the KFFE monomer described by the implicit solvent models EEF1, ACE, GB1, and GBSW. The energy scale (in kilocalories per mole) is given for each map on the right.

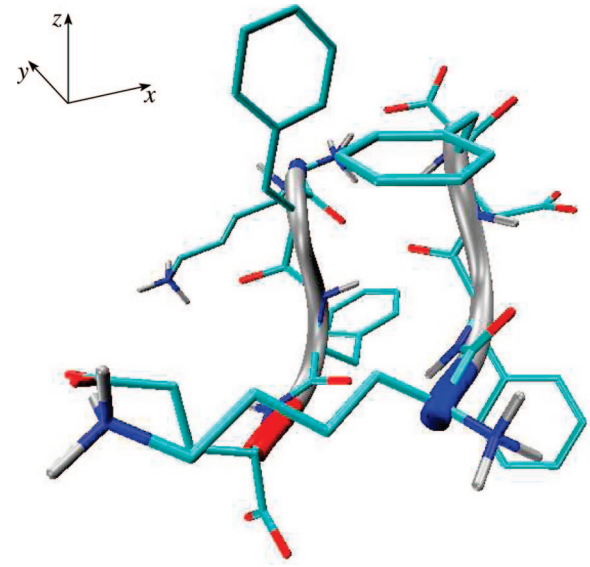

Figure 3. Reference antiparallel β-sheet structure for the KFFE dimer.

and C22 (GBSW) force fields is almost exclusively due to salt bridges between the oppositely charged Lys and Glu residues. This attraction is reduced by repulsive self-interactions arising from the double charges at the unblocked termini. Here, the united-atom force field C19 predicts a stronger repulsion for the negative C terminus than for the positive N terminus, whereas for the all-atom C22 force field the opposite is true. Given that at the N terminus the two positive charges are further apart than the two negative charges at the C terminus, one would expect a larger repulsion at the C terminus, as predicted by the C19 force field. The electrostatic attraction between the termini is also present in the in vacuo β-strand. It is, however, reduced due to the increased distance between them. The loss of intramolecular electrostatic interactions in the β-strand is compensated by electrostatic peptide−solvent interactions. The main difference in solvation energy for the β-strand and turn stems from the electrostatic, and not the nonpolar, contribution to ΔG_{solv}. The solvent accessible surface areas of these two structures are indeed very similar, namely 620 Å^2 for the β-strand and 580 Å^2 for the turn, and give rise to similar nonpolar solvation free energies in the range of 10−20 kcal mol^{-1}. The inclusion of charge screening in the C19E force field substantially changes the Coulomb interaction between the residues. The most pronounced difference from the in vacuo result is the greatly reduced stability of the salt bridges between the termini in the turn structure and their complete screening in the β-strand. Instead, the electrostatic interactions between neighboring residues become important, which are stronger than those between the spatially more distant terminal residues. Like the other two force fields C19 and C22, C19E predicts a repulsive self-interaction for the C terminus, but an attractive self-interaction for the N terminus. The attraction between like charges in aqueous solution could be explained by the stabilizing effect of the solvent-mediated hydrogen-bonded bridges between them, which could overcome the Coulombic repulsion.[71,72] However, a stabilization of 10 kcal mol^{-1}, as found for the NH_3^+–Lys interaction, seems excessive and it is known that for some relative orientations of like charged side chains the EEF1 model predicts an attraction that is too strong.[73]

3.2. KFFE Dimer. *Results from Global Optimization.* For each potential, six independent BH simulations, each starting from a random structure from an initial high-temperature run, were performed. For each of the six runs, a cascade of several BH searches, each consisting of 10 000 steps, was carried out. The first search was started at a temperature of 5000 K, which was gradually reduced after each step down to 250 K at the end of the run. The lowest energy structure from each run was then taken as the starting geometry for the next run and the temperature for the following BH runs was fixed with values ranging from 270 up to 400 K. Various combinations of dihedral angle moves and rigid body moves were applied in the following BH runs. If after three successive BH runs, no structure of lower energy was found and the BH searches were terminated. For each solvent model, at least three of the six BH runs located the same structure of lowest potential energy, which is therefore assumed to be the global potential minimum.

Several different structures with energies only 0.5−2 kcal mol^{-1} above the global potential minimum have been located for all four of the solvent models considered. For each potential the structure of the global potential minimum is shown (together with other structures from REMD) in Figure 5. These structures are quite different from each other. The EEF1 and GBSW models favor an antiparallel orientation for the two KFFE peptides, but only the EEF1 potential supports a low-lying sheetlike structure with a C_α-rmsd of 1.2 Å from the ideal antiparallel β-sheet shown in Figure 3. As for the monomer, the GBSW potential prefers the turn structure for the KFFE dimer, with a global potential minimum consisting of two turns aligned antiparallel. In the global potential minimum located for the GB1 solvent model the two peptides are also in turn conformations, but rotated

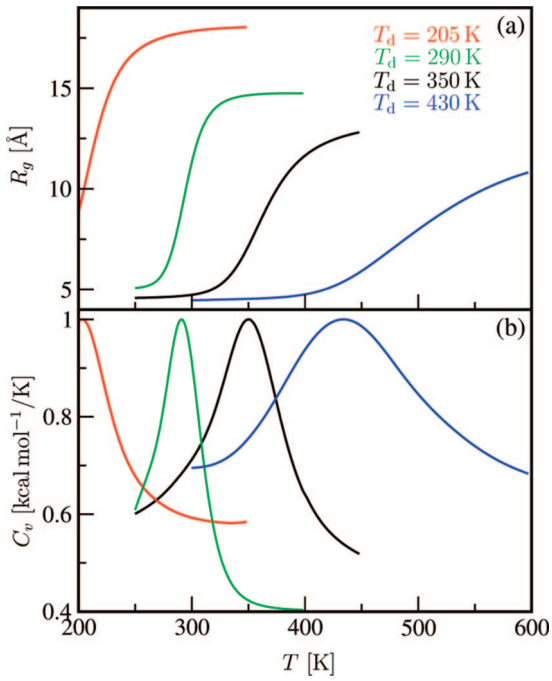

Figure 4. Temperature dependence of (a) the radius of gyration, R_g, and (b) the heat capacity, C_V, computed from replica exchange molecular dynamics simulations for the KFFE dimer described by the implicit solvent models EEF1 (black), ACE (red), GB1 (green), and GBSW (blue). The dissociation temperature, T_d, can be inferred from the peak in C_V and is given in panel a for each of the solvent models according to the color code. In the simulations, the peptides were confined to a spherical container with radius $R = 25$ Å.

relative to one another by about 90°. The global potential minimum for the ACE model consists of a β-strand and a turn with the C terminus of the strand pointing towards the middle of the turn. The dissimilarity of these four structures is further highlighted if one relaxes the global potential minimum from each solvent model using the other three potentials and then ranks their energies against that of the true global potential minimum. With one exception, the potential energies obtained always lie between 10 and 30 kcal mol^{-1} above the global potential minimum in question. The exception is the global minimum for GB1, which lies only 0.5 kcal mol^{-1} above the true global minimum for the GBSW solvation model, when relaxed with the latter force field.

REMD Simulations and Dissociation Temperature. All REMD simulations in implicit solvent were started by placing two KFFE peptides in random orientations for each replica. Before data collection, 20 000 MD steps were performed for equilibration, followed by a production phase of 100 ns at each temperature, involving 50 000 replica exchange cycles. The acceptance ratio for exchanges was uniform in the temperature range considered, with values between 0.35 and 0.5 for all REMD simulations. The temperature range for the REMD simulations was selected via short trial runs to ensure that the estimated dissociation temperature of the dimer, T_d, lay well within the interval in question. Specifically, T_{min} and T_{max} were set to 250 and 450 K for EEF1, 200 and 350 K for ACE, 250 and 400 K for GB1, and 300 and 600 K for GBSW. Eight independent replicas were considered for the GBSW potential and six replicas for the other three potentials. The principal quantities monitored during the REMD simulations were the total energy, E_{tot}, the peptide–peptide interaction energy, V_{int}, the radius of gyration, R_g, and the C_α-rmsd from the antiparallel β-sheet in Figure 3.

The heat capacity of the system, C_V, is plotted together with the radius of gyration, R_g, as a function of temperature in Figure 4. The dissociation temperature, T_d, can be inferred from the peak in C_V. Above this temperature R_g is controlled by the confining sphere as well as the equilibrium between the monomers and dimer. Figure 4a indicates that for higher dissociation temperatures the equilibrium is shifted toward the dimer, leading to lower values for R_g above T_d. For the four solvent models, we find dissociation temperatures of 350 K for EEF1, 205 K for ACE, 290 K for GB1, and 430 K for GBSW. Hence, the ACE potential shows the lowest propensity for aggregation and GBSW the highest.

In a similar REMD simulation of the KFFE dimer modeled by the GB1 potential, Baumketner and Shea found a dissociation temperature of 325 K.[31] The deviation of 35 K from our result can be explained by the smaller confining sphere, with $R = 17$ Å, used in their simulation compared to $R = 25$ Å in our study, as well as by the different temperature range chosen for the replicas. When we repeated the REMD simulation for the GB1 potential with exactly the same settings as in ref 31 we also found $T_d = 325$ K and obtained the same FES for $T = T_d$ as shown in Figure 2d of ref 31. With the larger container radius of $R = 25$ Å, the same representation for the FES, i.e., plotted as function of interaction energy between the KFFE peptides and R_g at the dissociation temperature $T_d = 290$ K, shows a greater free energy barrier for dimerization. Using an even larger container radius of $R = 43$ Å in the REMD simulations, which corresponds to a peptide concentration of 10 mM (still two orders of magnitude above the experimental concentration of 200−300 μM),[30] the ACE and GB1 potentials did not support a free energy minimum for the dimer. Hence, they clearly underestimate the aggregation propensity of KFFE. However, for the EEF1 and GBSW models the KFFE peptides still dimerize for container radii of 43 and 55 Å, the latter corresponding to a peptide concentration of 1 mM. The effect of the container radius on the dissociation temperature for the EEF1 potential is to produce a gradual decrease from $T_d = 365$ K for $R = 17$ Å to $T_d = 325$ K for $R = 55$ Å. Further studies will be needed to determine the effect of confinement on peptide aggregation. In the current work $R = 25$ Å was chosen as the default confining radius, since it allows aggregation to occur for each potential considered.

Structural Analysis of the Free Energy Minima. In Figure 5, the FES is plotted for the KFFE dimer as a function of R_g and the C_α-rmsd from the antiparallel β-sheet in Figure 3. Temperatures below T_d (300 K for EEF1, 200 K for ACE, 260 K for GB1, and 350 K for GBSW) were chosen for detailed analysis of the conformational space. Typical structures for the most populated free energy minima, along with the structure of the global potential minimum previously

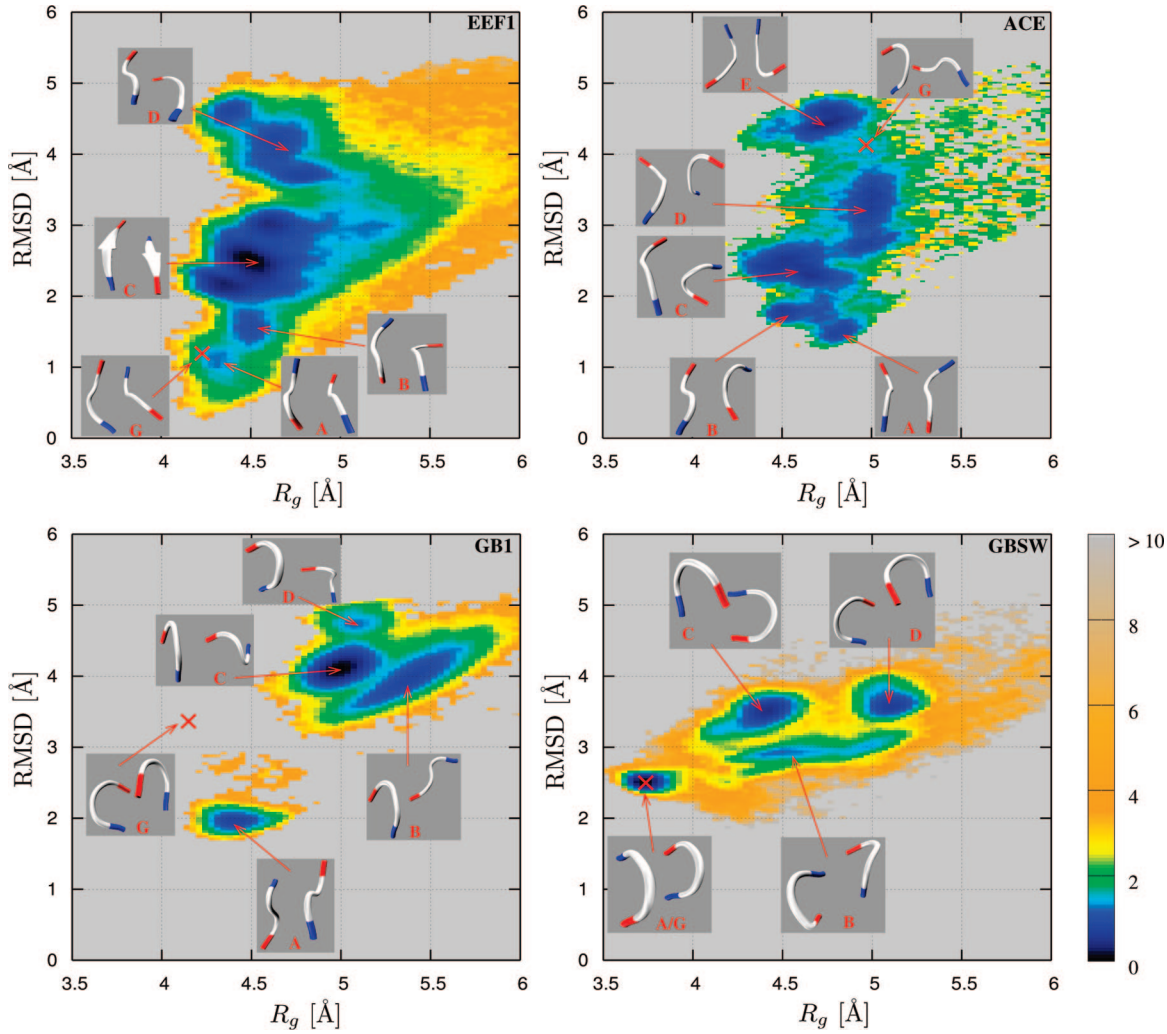

Figure 5. Free energy surfaces in terms of the radius of gyration, R_g, and C_α-rmsd from the ideal antiparallel β-sheet (Figure 3) for the KFFE dimer described by the implicit solvent models EEF1, ACE, GB1, and GBSW. The free energy surfaces are shown for temperatures below the dissociation temperature; specifically, $T = 300$ K for EEF1, 200 K for ACE, 260 K for GB1, and 350 K for GBSW. The energy scale (in kilocalories per mole) is given on the right. Typical structures for the free energy minima are shown and labeled A−E. The structure of the global potential minimum, labeled G, found from basin-hopping is also shown together with its location on the free energy surface.

found from BH, are also presented in Figure 5. All of the free energy minima for EEF1 consist of sheetlike structures, which are aligned in an antiparallel fashion, aside from conformation EEF1-D. The most favorable geometry is structure EEF1-C, which is a twisted β-sheet. The twist causes a rmsd deviation of 2.5 Å from the untwisted reference β-sheet. The global potential minimum, EEF1-G, almost coincides with the free energy minimum EEF1-A, suggesting that the conformational space of the KFFE dimer described by the EEF1 potential is dominated by potential energy rather than entropy.

The FES for the ACE potential is also dominated by structures involving β-strands and other extended conformations of the KFFE peptide. The structure closest to the antiparallel β-sheet is the free energy minimum ACE-A. In one of the free energy minima, ACE-E, the two peptides are aligned parallel, despite the repulsion resulting from the like charges being next to each other, which must be compensated by other effects. The FES for GB1 exhibits four well-defined minima. The structure of GB1-A is closest to the antiparallel β-sheet, but one of the strands is flipped over. The same structure was identified in the study of Baumketner and Shea.[31] The other three minima are quite loose, with $R_g \gtrsim 5$ Å, and consist of one KFFE peptide adopting a turn conformation and the other a strand geometry, which points with its C terminus toward the middle of the turn. The structure of the global potential minimum, GB1-G, which was also identified by Baumketner and Shea,[31] is far away from any free energy minimum. From the findings for the ACE and GB1 solvation models we conclude that for both potentials solvation and entropy have a large impact on the conformations populated by the KFFE dimer. All four minima of the FES for GBSW are composed of two KFFE peptides in turn conformations. This finding again reflects the very low β-propensity of the GBSW model for KFFE. The free energy minima differ in the relative orientation of the two turns. Minimum GBSW-A is also the global potential minimum where the two peptides are aligned antiparallel. The coincidence of the global potential minimum with a free energy minimum provides evidence that stable

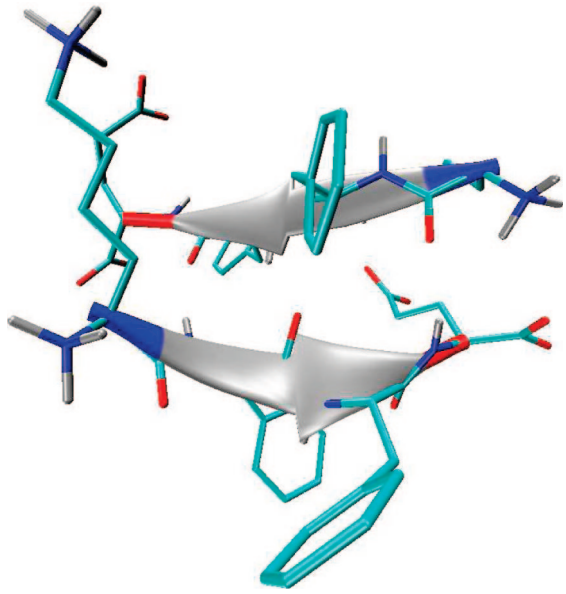

Figure 6. Twisted antiparallel β-sheet conformation found in replica exchange simulations of the KFFE dimer using the EEF1 implicit solvent model. It is referred to as structure EEF1-C.

KFFE dimers are populated, and it explains the high dissociation temperature found from the REMD simulation for GBSW.

Energy Analysis for the Free Energy Minima. To shed more light on how the intrapeptide, interpeptide, and peptide−solvent interactions trigger aggregation, all the structures presented in Figure 5 have been relaxed to local potential energy minima. The resulting total potential energies, E_{tot}, were decomposed into the following contributions: $V_{vac,1}$ and $V_{vac,2}$ for the intramolecular vacuum potential energies of the two KFFE peptides, V_{int} for the peptide−peptide interaction energy, and the solvation free energy, ΔG_{solv}. The results of this decomposition scheme are presented in Figure 7 for the relevant structures, as well as for the twisted antiparallel β-sheet, structure EEF1-C, which is shown in more detail in Figure 6. Based on experimental findings, this conformation should be the structural element of the KFFE amyloid fibril,[30] and we wish to understand why it is disfavored by the GB models under consideration. The five structures derived from the EEF1 potential are all very similar and are stabilized by the same forces. Solvation (excluding the screening of the peptide charges) always contributes about 45% to the total energy, and the other 55% is equally distributed between intra- and intermolecular terms. The results are not as straightforward for ACE and GB1. Most of the corresponding free energy minima are not very well stabilized by peptide−peptide interactions and are instead optimized for solvation. Exceptions are the structures ACE-B and ACE-C, for which V_{int} contributes about 25% to E_{tot}. However, these structures are in equilibrium with the three other free energy minima, which are only marginally or not at all stabilized by V_{int}, and thus can easily dissociate. That the peptide−peptide interaction is not a strong driving force for aggregation for ACE can also be seen for the global potential minimum, where solvation contributes 53% and V_{int} only 10% to E_{tot}. The antiparallel β-sheet, on the other hand, is significantly stabilized by the interaction between the two strands, yet is clearly disfavored by the ACE solvation energy. The same findings as for the structures ACE-A through ACE-E apply for the structures GB1-A through GB1-D, i.e., they are stabilized by solvation rather than the peptide−peptide interaction and are thus susceptible to dissociation. For the global potential minimum GB1-G, on the other hand, V_{int} contributes 34% to E_{tot}, but this structure is clearly disfavored by solvation and entropy. A similar picture holds for the EEF1-C structure when described by the GB1 potential. The GBSW structures are all stabilized by peptide−peptide interactions and by the solvation energy, leading to stable KFFE dimers. As already found in the study of the KFFE monomer, the peptides alone are quite unstable, with either small negative or even positive values for the energies $V_{vac,i}$. These destabilizing forces are due to the large electrostatic repulsion at the charged termini within the C22 force field. They are most destabilizing for the β-conformation of the KFFE peptide, thus preventing the antiparallel β-sheet from forming within the GBSW description.

Residue–Residue Interactions in the β-Sheet. The peptide−peptide interactions present in the twisted β-sheet in Figure 6 can be decomposed into electrostatic, V_{int}^{el}, and vdW, V_{int}^{vdW}, contributions, which are listed in Table 2. For each potential the vdW interactions are less stabilizing than the electrostatic forces. The unscreened β-sheet is dominated by attractive Coulomb interactions arising from the salt bridges between the unblocked Lys and Glu residues from adjacent strands. However, after the inclusion of screening due to the solvent, one finds that V_{int}^{vdW} is of a similar magnitude to V_{int}^{el}, as the result for EEF1 shows. The comparison of V_{int}^{el} between the C19E and C19 force fields reveals that the solvent reduces the electrostatic interpeptide interactions by 220−230 kcal mol^{-1}. If one assumes the same amount of screening for the GBSW solvent model, the Coulomb interactions would remain three or four times more important for the β-sheet described by the C22 force field.

Analysis of the vdW interactions is of interest to help answer questions about the importance of the $\pi-\pi$ interactions between the Phe residues in adjacent strands.[30] To this end, we have decomposed V_{int}^{vdW} into its residue−residue contributions, and the results are presented in Figure 8. Since there is no difference in the description of the vdW interactions between the C19 and C19E force fields, and since the equilibrated structures of the EEF1-C β-sheet differ only marginally for EEF1, ACE, and GB1, we show only one residue−residue map representing the C19(E) force fields and another one for the C22 force field from the GBSW calculation. The comparison between these two plots reveals that the vdW interactions are quite different. For instance, with the C19(E) force fields the most stabilizing interaction is between Lys and Glu, with a value of –5.0 kcal mol^{-1}. The same residue pairing gives a repulsive vdW interaction of 2.5 kcal mol^{-1} for the C22 force field and instead finds the strongest such interactions for the Phe−Lys and Phe−Phe pairs with values of –2.5 kcal mol^{-1}. From the results in Figure 8, we conclude that $\pi-\pi$ interactions

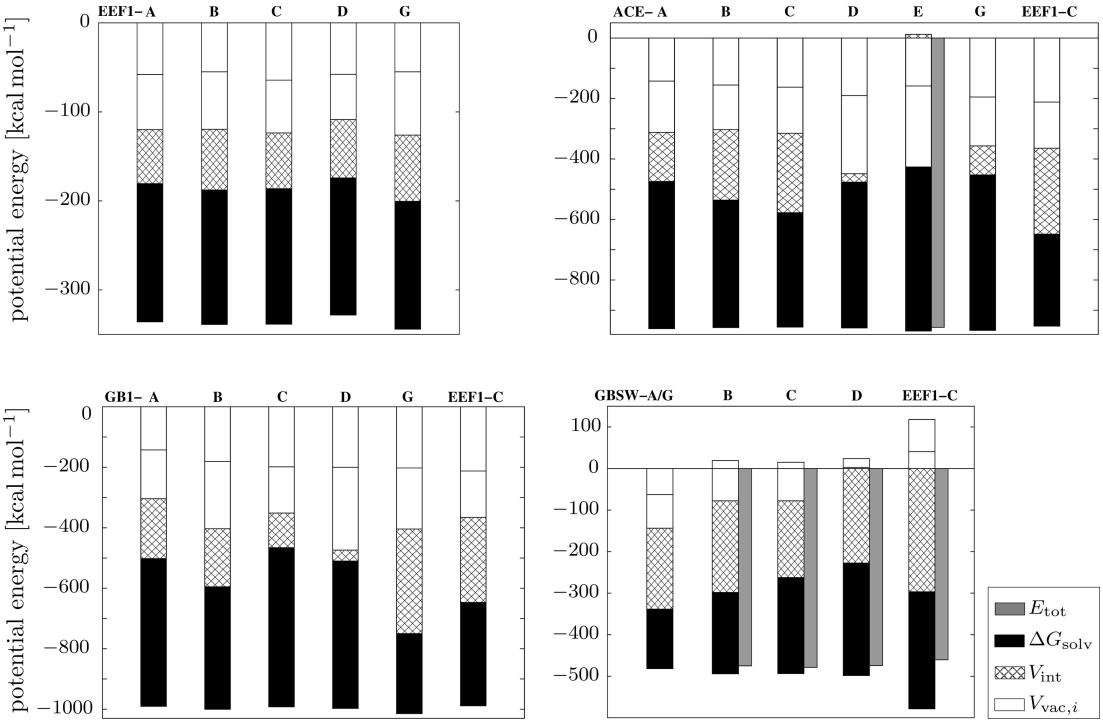

Figure 7. Energy contributions to the EEF1-C β-sheet (Figure 6) for the implicit solvent models EEF1, ACE, GB1, and GBSW. The total potential energy, E_{tot}, is decomposed into the vacuum energies, $V_{vac,i}$, of the two KFFE peptides, their interaction energy, V_{int}, and the solvation free energy, ΔG_{solv}. If one of the contributions is positive, E_{tot} is plotted explicitly, otherwise it is $E_{tot} = V_{vac,1} + V_{vac,2} + V_{int} + \Delta G_{solv}$.

Table 2. Contributions to the Interaction Energy, V_{int}, between the KFFE Peptides in the twisted β-Sheet (Figure 6)[a]

	V_{int}^{el}	V_{int}^{vdW}
EEF1[a]	−34.5	−28.1
ACE	−252.3	−31.7
GB1	−250.3	−31.5
GBSW	−282.3	−14.4

[a] The electrostatic energies, V_{int}^{el}, are not really vacuum values for the EEF1 potential, because the C19E force field has charge screening incorporated into its parameters.

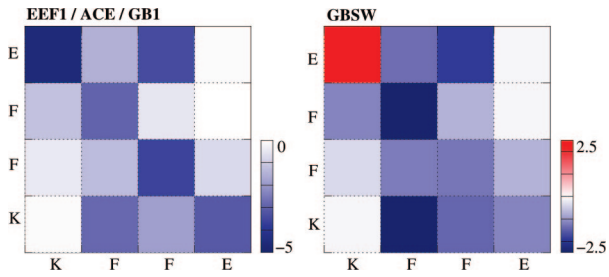

Figure 8. Residue–residue map of the van der Waals interaction energy between the two KFFE peptides in the EEF1-C β-sheet (Figure 6). The map on the left shows the result for the CHARMM19 force field used together with EEF1, ACE, and GB1 solvent models. The map on the right shows the result for the CHARMM22 force field used together with the GBSW solvent model. The energy scale (in kilocalories per mole) is given for both maps on the right.

play a role in the stabilization of the antiparallel β-sheet for KFFE, but are not more important than other vdW interactions.

4. Discussion and Conclusions

The process of aggregation is a delicate balance between the competing solvation forces and intra- and intermolecular forces. In the case of the KFFE peptide this competition is seen experimentally from the following results.[30] (i) If one removes the terminal charges of the unblocked KFFE peptide by acetylating the N terminus and amidating the C terminus the fibril formation is significantly reduced. (ii) KFFK and EFFE do not form fibrils when incubated individually, but aggregate when incubated together in equimolar concentrations. (iii) KFFE and KVVE form amyloid fibrils whereas KLLE and KAAE do not. These findings reveal that charge attraction plays a crucial role for fibril formation. However, Coulombic forces are not the only factor governing amyloid aggregation, otherwise KLLE and KAAE should also form fibrils. Other factors include the β-propensity and hydrophobic interactions. The KFFE and KVVE peptides show partial β-conformations in solution, whereas KLLE and KAAE do not.[30] KFFE is also the most hydrophobic peptide and KAAE the least from the four peptides studied experimentally. The objective of any theoretical model would be to reproduce these experimental findings and explain them in atomistic detail. However, most of the empirical potentials that allow us to study such peptides including solvent effects in a reasonable length of time, have certain shortcomings leading to an imbalanced description of the aggregation process.

The EEF1 potential produces results that are closest to the experimental findings of partial β-strand conformation for the KFFE peptide in solution and the formation of fibrils exhibiting β-strand structure.[30] Thus, of the four energy

functions considered, the EEF1 potential provides the best balanced description for the secondary structure of the KFFE peptide and the detailed interplay between solvation forces and intermolecular forces. Other advantages of the EEF1 energy function are that it is very fast to evaluate and numerically stable. Our conclusion is in line with other comparative studies assessing the performance of various implicit solvent models implemented in CHARMM, which also also found that the EEF1 model is one of the most reliable potentials in identifying experimental structures or minima from explicit solvent simulations.[21,28] The success of the EEF1 potential in describing protein aggregation probably lies in incorporating the solvent screening by reducing the side chain charges. The resulting C19E parameters are also used together with the implicit solvent model SASA, which is based on the solvent-accessible surface area to describe the main effects of the aqueous solvent on the solute.[25] This potential has recently been used in MD simulations of various amyloidogenic peptides to predict aggregation pathways and the resulting β-sheet structures,[37,74,75] and to identify β-aggregation "hotspots" in amyloidogenic proteins.[38] It correctly predicted the in-register parallel packing of three GNNQQNY peptides,[37] whereas when applied to polypeptide sequences experimentally known not to form amyloid structures no ordered β-aggregates were observed.[37,74]

The main limitation of the EEF1 solvent model that we are aware of, is the empirical implementation of the charge screening by neutralizing the charged termini and sidechains. While in many cases this approximation gives reasonable results, in some instances the Coulomb interaction between charges is underestimated. This failure is most pronounced for repulsive interactions between like charges, which the EEF1 solvent model often predicts to be attractive as, for example, in the interaction between the two positive charges in the unblocked N terminus of KFFE (Figure 2). This issue has already been addressed by Masunov and Lazaridis in a study of the interactions between ionizable amino acid side chains.[73] In a recent study of protein−surface interactions, EEF1 also overestimated the electrostatic screening for a negatively charged peptide approaching a negatively charged surface.[29] A possible way to address this problem could be to derive the partial charges for the amino acids from electronic structure calculations combined with an implicit solvent model.

The ACE and GB1 models predict similar results for both the KFFE monomer and dimer due to the similarity of the two potentials. Both solvent models were used together with the C19 force field and both GB models use a pairwise approach summing over atomic volumes to approximate the volume integral (3) for the calculation of the effective Born radii within the CFA. The ACE and GB1 potentials predict a similar β-propensity for the KFFE peptide as EEF1, but fail to produce stable KFFE dimers. It seems that the balance between the competing forces triggering aggregation lies in favor of solvation, preventing stable dimers from forming and thus underestimating the aggregation propensity. The two KFFE peptides can be forced to form a dimer by confining them into a rather small sphere, which still results in a dissociation temperature well below the experimental value. The comparison between the EEF1 and ACE/GB1 results reveal that a similar description of the conformational space of a single peptide does not guarantee the same behavior of the potentials with respect to peptide aggregation.

The overestimation of solvation energies for ACE and GB1 contrasts with the common assumption that GB models based on the CFA tend to underestimate the solvation energy, due to an overestimation of the effective Born radii compared to the exact ones calculated by solving the PB equation.[10] However, in a previous comparison it was found that the performance of a GB method also varies with the conformation of the protein.[76] For a test set of 120 near-native, misfolded and unfolded structures of chicken villin headpiece, GB1 (used together with C22) overestimates the solvation energy for extended structures, while the solvation energies for nativelike conformations are not favorable enough. This finding would explain our observation that the extended KFFE peptide does not form stable dimers and instead prefers solvent exposed configurations for GB1. The results for the ACE solvent model published in ref 76 do not support our finding of an overestimation of the solvation energy for the extended KFFE peptide. However, in ref 76 the ACE model was used together with C22 and a new parameter set with zero hydrogen volumes. Hence the ACE models in our study and in ref 76 may be too different to produce consistent results. Our conclusions are supported by two other studies (using the C19 force field), which both find that salt bridges are screened too much within the ACE potential,[27,29] and that charged residues prefer solvent exposed orientations for ACE and GB1.[27] It is not clear whether this failure is due to the ACE and GB1 solvent models or to the in vacuo performance of the C19 force field.

The GBSW model supports a very stable antiparallel dimer structure, but with the KFFE peptides in a turn rather than a β conformation. Compared to experiment, GBSW clearly disfavors the β-state, which can be attributed to an overestimation of the electrostatic forces present in the KFFE peptide. The effective electrostatic forces are stronger than the CMAP corrections to the C22 potential. Thus it is unlikely that further corrections to the backbone dihedral cross terms, as introduced recently for the CHARMM22/CMAP/GBSW potential, would change the current result.[77] For the uncapped KFFE peptide modeled by the C22 potential, significant repulsive forces are found at the doubly charged termini. In the turn structure, these repulsions are more than compensated by attraction between the adjacent N and C termini. In the β-strand, however, the termini are too far apart from each other to counteract these repulsions. The apparently excessive Coulomb forces could be due to either an overestimation of the partial charges in the ionizable side chains and termini in the C22 force fields, or to an underestimation of the charge screening by GBSW. We have found several indications to support the former possibility. (i) We have checked that the GBSW result for the KFFE monomer does not change if the terminal charges are further screened by invoking the GBSW solvent model with a salt concentration of 0.05 and 5.0 M, or if they are removed by acetylating the N terminus and amidating the C terminus. In

each case the β-strand remains substantially disfavored. (ii) From the study in ref 76 it is known that GBSW tends to overestimate the solvation energy for extended structures,[76] which should favor the β-strand for the KFFE peptide, but not the turn. (iii) A 50 ns REMD simulation of the KFFE dimer using the TIP3P explicit water model,[26] combined with the C22 force field, produces an FES similar to that from the GBSW simulation. Details of this simulation are given in Appendix B. The only difference is that minima GBSW-A and GBSW-C are less populated in the explicit water simulation. From these results we conclude that the partial charges for the charged termini and side chains in the C22 force field are probably overestimated, rather than the screening by GBSW being underestimated. An adjustment of these charges could be beneficial for both the performance of the C22 force field and for GBSW, as well as for other GB solvent models. However, we acknowledge that the calibration of a force field is a complex process and the change of partial charges would entail extensive reparametrization of the force field. We finally note that the GBSW solvent model is computationally less efficient compared to EEF1, but also compared to ACE and GB1, due to the numerical evaluation of the integral in eq 3. In addition, we observed that the default values for the number of grid points in the numerical integration do not produce well converged results, as discussed in Appendix C.

The nonelectrostatic interactions, such as dispersion, between the two KFFE peptides in the antiparallel β-sheet are described quite differently by the C19(E) and C22 force fields, as shown in Figure 8. For instance, the most attractive vdW force between Lys and Glu for the C19(E) potential is repulsive for C22. In both energy functions the $\pi-\pi$ interaction between phenylalanines is no more stabilizing than other vdW interactions. Hence, the present force fields do not suggest a dominant role for π interactions in amyloid formation.[78] However, it is known from experiment that charge attraction is not the only factor in the aggregation process, as the comparative study of KFFE, KVVE, KLLE, and KAAE shows.[30] Interestingly, the more hydrophobic KLLE does not form fibrils while KVVE does. To resolve such subtleties, and to quantify the impact of hydrophobicity and β-propensity on the aggregation process, more accurate potentials are probably needed. A comparison between the results from ab initio electronic structure calculations and empirical potentials would be helpful to reliably identify the most stabilizing forces in the different dimers. However, such calculations involving intermolecular interactions have to be performed with care, especially if accurate treatment of dispersion is required.

Our results allow us to infer the likely behavior of the various force fields and solvent models in describing the aggregation processes of the KFFE peptide beyond dimerization, although we have only studied the latter process in the present contribution. The structure of the KFFE dimer is not yet known experimentally and it is not clear whether it serves as a nucleation site for fibrillization, or whether it rather represents an off-pathway kinetic intermediate. Based on our results it seems unlikely that stable amyloid fibrils would be obtained for KFFE described by the C22 force field/GBSW solvent model, due to the very low β-propensity in this case. The C19 force field combined with the ACE and GB1 solvent models, on the other hand, clearly underestimate the aggregation propensity of the KFFE peptide. Thus out of the four potentials in question, EEF1 is probably the most promising representation of the KFFE peptide and its aqueous surroundings for future studies of the oligomerization processes beyond dimerization, which eventually lead to fibrillization.

Acknowledgment. The authors are grateful to Dr J.-E. Shea and Dr A. Baumketner for providing us with the structures of the KFFE dimer from their theoretical study for comparison. B.S. gratefully acknowledges the BBSRC for financial support.

Appendix A. Solvent Models

EEF1. The EEF1 model is a solvent-exclusion model based on the assumption that the solvation free energy of a protein is a sum of group contributions, which are determined from values for small, fully solvent-exposed model compounds minus the reduction in solvation because of the presence of surrounding groups:

$$\Delta G_{\mathrm{solv}} = \sum_i \Delta G^{\mathrm{ref}}_{\mathrm{solv},i} - \sum_i \sum_{j \neq i} f_i(r_{ij}) V_j \tag{6}$$

Here, $\Delta G^{\mathrm{ref}}_{\mathrm{solv},i}$ is the solvation free energy of the reference compound i, r_{ij} is the distance between i and j, V_j is the volume of group j, and $f_i(r_{ij})$ is the solvation free energy density, which is assumed to be a Gaussian function. To account for the screening of the interactions between charges due to the solvent, ordinarily charged protein groups (ionic side chains and termini) are neutralized and a distance-dependent dielectric constant is employed. The EEF1 model was used together with a modified version of the united-atom CHARMM19 parameters, which contain the neutralized side chains and termini. For the calculation of the nonbonded interactions, the same cutoffs were used for which the EEF1 model was parametrized, i.e., both vdW and electrostatic interactions were cut off at 9 Å with a switching function between 7 and 9 Å.

GB1. The GB method, which we refer to here as GB1, follows the pairwise approach, summing over atomic volumes to approximate the volume integral (3) for the calculation of the Born radii. It uses a linearized version of Still's original formula[4] for the self-electrostatic free energy of atom i,[15]

$$\Delta G_{\mathrm{el},i} = \tau \left[\frac{1}{\lambda}\left(\frac{-166}{R_i}\right) + P_1\left(\frac{166}{R_i^2}\right) + \sum_j^{\mathrm{bond}} \frac{P_2 V_j}{r_{ij}^4} + \sum_j^{\mathrm{angle}} \frac{P_3 V_j}{r_{ij}^4} + \sum_j^{\mathrm{nonbond}} \frac{P_4 V_j C}{r_{ij}^4} \right] \tag{7}$$

where $V_j = 4/3\pi R_j^3$ is the atomic volume of atom j and C is a close-contact function that adjusts radii for nonbonded atoms close to atom i. The reduction of atomic volumes due to neighboring atoms is accounted for by the adjustable parameters γ and P_k, which were refitted by Dominy and Brooks to solvation energies from PB calculations for a

database of peptides.[15] As in the study by Baumketner and Shea,[31] we used GB1 together with the CHARMM19 parameters and no truncation of the nonbonded interactions was performed.

ACE. In their GB implementation, Schaefer and Karplus developed an analytical and continuous pairwise atomic expression for the electrostatic solvation energy, which is known as the analytical treatment of continuum electrostatics (ACE).[7] In the ACE model, the volume integral over the solute in eq 3 is rewritten as an integral over all space and the integrand is multiplied by a step function, $P(\mathbf{r})$, whose value is one in the solute's interior and zero elsewhere. This function can be expressed as a sum of atomic terms, $P(\mathbf{r}) = \Sigma_i P_i(\mathbf{r})$, and the density functions $P_i(\mathbf{r})$ describing the atomic volume are given by Gaussians, whose width and height control the smoothness of the atomistic solute volume description. The resulting expression for the self-electrostatic energy is

$$\Delta G_{el,i} = -\frac{\tau q_i^2}{2R_i} + \sum_{j\neq i} \frac{\tau q_i^2}{\omega_{ij}} \exp(-r_{ij}^2/\sigma_{ij}^2) + \frac{\tau q_i^2 \tilde{V}_j}{8\pi} \left(\frac{r_{ij}^3}{r_{ij}^4 + \mu_{ij}^4} \right)^4 \tag{8}$$

where the parameters ω_{ij} and σ_{ij} determine the width and height of the Gaussian, which dominates $\Delta G_{el,i}$ in the short-range domain. At long-range $\Delta G_{el,i}$ is dominated by the last term in eq 8, which vanishes for $r_{ij} = 0$ due to the parameter μ_{ij}. For the volumes $\tilde{V}_j$ we used the parameter set based on the Voronoi volumes for the CHARMM19 force field,[79] which we employed together with the ACE solvent model. The calculation of the nonbonding interactions was performed without a cutoff.

GBSW. The GBSW model[11] is one of the most recent GB models and involves a continuous and smooth switching function to define the molecular surface. To improve the calculated Born radii, an empirical correction term, $\Delta G^1_{el,i}$, is added to the Coulomb field term, $\Delta G^0_{el,i}$.[10] The self-electrostatic free energy can then be expressed as

$$\begin{aligned} \Delta G^1_{el,i} &= a_0 \Delta G^0_{el,i} + a_1 \Delta G^1_{el,i} \\ &= -\frac{\tau q_i^2}{2} \left[a_0 \left(\frac{1}{R_i} - \frac{1}{4\pi} \int_{\text{solute},r>R_i} \frac{1}{r^4}\, dV \right) + \right. \\ &\qquad \left. a_1 \left(\frac{1}{R_i^4} - \frac{1}{4\pi} \int_{\text{solute},r>R_i} \frac{1}{r^7}\, dV \right)^4 \right] \end{aligned} \tag{9}$$

from which the Born radii can be calculated according to eq 3. The volume integrals in eq 9 are evaluated numerically using Gaussian-Legendre quadrature[80] for the radial grid points and Lebedev quadrature[81] for the angular grid points. For each atom, we used 50 angular integration points and 24 radial integration points up to 20 Å. For the switching function at the dielectric boundary, we chose a smoothing length of 0.6 Å and used the values $a_0 = -0.180$ and $a_1 = -1.817$ for the coefficients in (9), as recommended for this choice of smoothing length.[11] We employed GBSW together with the CHARMM22 force field including the CMAP modifications,[48–50] and the nonbonded interactions were calculated without cutoffs.

Appendix B. Details of the REMD Simulation with TIP3P Water

The TIP3P water model[26] was used together with the CHARMM22/CMAP force field. The peptides were solvated in a preequilibrated cubic box of TIP3P water molecules extending at least 10 Å from any solute atom. Any water molecule that was too close to the peptides, i.e. within 2 Å, was removed. The solvated system was initially minimized for 4000 steps using the adapted basis Newton-Raphson algorithm[80] to remove any bad contacts. The minimized system was gradually heated from 50 to 700 K in 20 K increments using short 10 ps MD runs. During heating, the backbone atoms of the peptides were restrained to their initial positions with a force constant of 5 kcal mol^{-1} to allow relaxation of the water molecules. All MD simulations with TIP3P employed the SHAKE algorithm,[64,65] with a geometric tolerance of 0.0001 Å to constrain covalent bonds involving hydrogen atoms, thus allowing a time step of 2 fs in the verlocity Verlet algorithm[82,83] to integrate Newton's equations. For MD runs at constant temperature, the *NVT* ensemble was used together with the Nose-Hoover thermostat.[84] For the nonbonding interactions a cutoff of 10 Å was used, while vdW interactions were switched to zero between 7 and 9 Å, and the particle-mesh Ewald technique was employed to calculate the long-ranged electrostatic energies along with a force-shifting function at a cutoff distance of 9 Å.[85,86]

The edge length of the cubic water box was chosen to be 40.6 Å, yielding a total of 2130 water molecules, which corresponds to the same peptide concentration of 50 mM as in the implicit solvent runs. For the initialization of the REMD simulation, a random conformation for the KFFE dimer was chosen followed by solvation, minimization and gradual heating. Every 20 K the structure was saved and taken as the starting point for the replica that was closest in temperature. The REMD simulation consisted of 32 replicas, with temperatures exponentially spaced between 300 and 600 K. Prior to the production phase, each replica was allowed to further equilibrate in a 5 ns MD run. During the subsequent production phase, 25 000 replica exchange cycles of 2 ps length were applied, resulting in a total production length of 50 ns at each temperature. The acceptance ratio was found to be quite uniform throughout the considered temperature range with values between 0.1 and 0.25.

Appendix C. Numerical Convergence of the GBSW Solvent Model

When performing global optimization and minimization of structures with the GBSW potential, we became aware of convergence problems arising from the numerical volume integration for the calculation of the Born radii. The recommended values are 24 radial grid points for the Gaussian-Legendre quadrature and 38 angular grid points for the Lebedev quadrature.[11] However, these values do not seem to give well converged energies for our purposes in the present system, as demonstrated in Figure 9 for the antiparallel β-sheet of the KFFE dimer shown in Figure 3. This structure was rotated around the x-axis in increments of 10° up to 90° and the energy before and after minimization

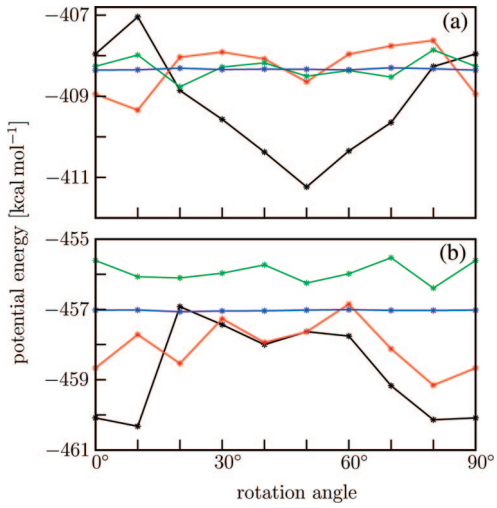

Figure 9. Convergence behaviour of the GBSW solvent model is analyzed for the ideal β-sheet of the KFFE dimer (Figure 3). This structure was rotated around the *x*-axis from 0° up to 90° in increments of 10° and the energy was calculated (a) before and (b) after minimization using the GBSW implicit solvent model with 24 radial grid points and 38 (black), 50 (red), 110 (green), and 590 (blue) angular Lebedev grid points.

was calculated using 24 radial grid points and 38, 50, 110, and 590 angular grid points.[81] It can be seen in Figure 9b that after minimization the energy varies by more than 4 kcal mol^{-1} for the default value of 38 angular grid points and by more than 2 kcal mol^{-1} for 50 Lebedev grid points. The resulting minimized structures are also different from each other. Another problem is that the energy variations before and after minimization are not correlated, i.e. orientations with high energies before minimization can become lowest in energy after minimization, and vice versa, as the comparison between Figure 9a and b reveals. The results improve on increasing the number of Lebedev grid points, with energies varying less than 1 kcal mol^{-1} for 110 and less than 0.1 kcal mol^{-1} for 590 grid points. However, for methods that rely on the unambiguous identification of stationary points of the potential energy surface, such as discrete path sampling,[87,88] even a set of 590 angular grid points does not give sufficiently converged results. Furthermore, the KFFE dimer with 160 atoms is a rather small system, and the magnitude of the energy variation with orientation scales linearly with increasing system size. For this reason, and because of the linear scaling of the computer time required for volume integration with the number of integration points and atoms, the solution to this problem probably does not lie in increasing the number of integration points. We note that these issues are probably unimportant in conventional Monte Carlo or molecular dynamics simulations.

For calculations that do not require energy gradients, we could simply orient the angular integration grid so that the Cartesian axes coincide with the principal axes of the molecule. This approach provides a rotationally invariant energy, but not the correct gradients. The calculation of solvation forces becomes more complicated because the integration points $\mathbf{r}_{mn}$ in eqs 23 and 24 in ref 11 are now dependent on all the atomic positions, and the calculation of the derivatives of the integration points $\mathbf{r}_{mn}$ with respect to each atom α would be necessary. The dependence of the integration points $\mathbf{r}_{mn}$ on the atomic positions $\{\mathbf{r}_\alpha\}$ results from the diagonalization of the inertia tensor of the molecule to obtain the rotation matrix that orients the angular grid points with respect to the principal axes. Hence, the derivatives $\partial\mathbf{r}_{mn}/\mathbf{r}_\alpha$are quite involved, and we have not pursued the option of orienting the grid. If precisely converged stationary points are required, it may be better to replace the numerical volume integration with an analytical implementation, as in the parameter-free pairwise descreening GB models,[5,6] while keeping the correction to the Coulomb field approximation.[6,10,13] Such an approach also has the advantage that the evaluation of the Born radii would probably be faster than the current implementation based on numerical integration.

References

(1) Chen, J.; Brooks, C. L., III *Phys. Chem. Chem. Phys.* **2008**, *10*, 471–481.

(2) Still, W. C.; Tempczyk, A.; Hawley, R. C.; Hendrickson, T. *J. Am. Chem. Soc.* **1990**, *112*, 6127–6129.

(3) Hawkins, G. D.; Cramer, C. J.; Truhlar, D. G. *Chem. Phys. Lett.* **1995**, *246*, 122–129.

(4) Qiu, D.; Shenkin, P. S.; Hollinger, F. P.; Still, W. C. *J. Phys. Chem. A* **1997**, *101*, 3005–3014.

(5) Gallicchio, E.; Levy, R. M. *J. Comput. Chem.* **2004**, *25*, 479–499.

(6) Tjong, H.; Zhou, H.-X. *J. Phys. Chem. B* **2007**, *111*, 3055–3061.

(7) Schaefer, M.; Karplus, M. *J. Phys. Chem.* **1996**, *100*, 1578–1599.

(8) Ghosh, A.; Rapp, C. S.; Friesner, R. A. *J. Phys. Chem. B* **1998**, *102*, 10983–10990.

(9) Scarsi, M.; Apostolakis, J.; Caflisch, A. *J. Phys. Chem. A* **1997**, *101*, 8098–8106.

(10) Lee, M. S.; Salsbury, F. R.; Brooks, C. L. *J. Chem. Phys.* **2002**, *116*, 10606–10614.

(11) Im, W.; Lee, M. S.; Brooks, C. L. *J. Comput. Chem.* **2003**, *24*, 1691–1702.

(12) Lee, M. S.; Feig, M.; Salsbury, F. R.; Brooks, C. L. *J. Comput. Chem.* **2003**, *24*, 1348–1356.

(13) Grycuk, T. *J. Chem. Phys.* **2003**, *119*, 4817–4826.

(14) Brooks, B. R.; Bruccoleri, R. E.; Olafson, B. D.; States, D. J.; Swaminathan, S.; Karplus, M. *J. Comput. Chem.* **1983**, *4*, 187–217.

(15) Dominy, B. N.; Brooks, C. L. *J. Phys. Chem. B* **1999**, *103*, 3765–3773.

(16) Dominy, B. N.; Brooks, C. L. *J. Comput. Chem.* **2001**, *23*, 147–160.

(17) Feig, M.; Brooks, C. L. *Proteins* **2002**, *49*, 232–245.

(18) Felts, A. K.; Gallicchio, E.; Wallqvist, A.; Levy, R. M. *Proteins* **2002**, *48*, 404–422.

(19) Zhu, J.; Zhu, Q.; Shi, Y.; Liu, H. *Proteins* **2003**, *52*, 598–608.

(20) Fiser, A.; Feig, M.; Brooks, C. L.; Sali, A. *Acc. Chem. Res.* **2002**, *35*, 413–421.

(21) Steinbach, P. J. *Prot. Struct. Func. Bioinf.* **2004**, *57*, 665–677.

(22) Bursulaya, B. D.; Brooks, C. L. *J. Phys. Chem. B* **2000**, *104*, 12378–12383.

(23) Karanicolas, J.; Brooks, C. L. *Proc. Natl. Acad. Sci. USA* **2004**, *101*, 3432–3437.

(24) Ohkubo, Y. Z.; Brooks, C. L. *Proc. Natl. Acad. Sci. USA* **2003**, *100*, 13916–13921.

(25) Ferrara, P.; Apostolakis, J.; Caflisch, A. *Proteins: Struct., Func., Gen.* **2002**, *46*, 24–33.

(26) Jorgensen, W. L.; Chandrasekhar, J.; Madura, J. D.; Impey, R. W.; Klein, M. L. *J. Chem. Phys.* **1983**, *79*, 926–935.

(27) Stultz, C. M. *J. Chem. Phys B* **2004**, *108*, 16525–16532.

(28) Huang, A.; Stultz, C. M. *Biophys. J.* **2007**, *92*, 34–45.

(29) Sun, Y.; Latour, R. A. *J. Comput. Chem.* **2006**, *27*, 1908–1922.

(30) Tjernberg, L.; Hosia, W.; Bark, N.; Thyberg, J.; Johansson, J. *J. Biol. Chem.* **2002**, *277*, 43243–43246.

(31) Baumketner, A.; Shea, J.-E. *Biophys. J.* **2005**, *89*, 1493–1503.

(32) Wei, G.; Mousseau, N.; Derreumaux, P. *J. Phys. Cond. Mat.* **2004**, *16*, 5047–5054.

(33) Wei, G.; Mousseau, N.; Derreumaux, P. *Biophys. J.* **2004**, *87*, 3648–3656.

(34) Melquiond, A.; Boucher, G.; Mousseau, N.; Derreumaux, P. *J. Chem. Phys.* **2005**, *122*, 174904.

(35) Melquiond, A.; Mousseau, N.; Derreumaux, P. *Prot. Struct. Func. Bioinf.* **2006**, *65*, 180–191.

(36) Meinke, J. H.; Hansmann, U. H. E. *J. Chem. Phys.* **2007**, *126*, 014706.

(37) Gsponer, J.; Haberthür, U.; Caflisch, A. *Proc. Natl. Acad. Sci. USA* **2003**, *100*, 5154–5159.

(38) Cecchini, M.; Curcio, R.; Pappalardo, M. M.; Melki, R.; Caflisch, A. *J. Mol. Biol.* **2006**, *357*, 1306–1321.

(39) Strodel, B.; Whittleston, C. S.; Wales, D. J. *J. Am. Chem. Soc.* **2007**, *129*, 16005–16014.

(40) Wales, D. J.; Doye, J. P. K. *J. Phys. Chem. A* **1997**, *101*, 5111–5116.

(41) Doye, J. P. K.; Wales, D. J. *Phys. Rev. Lett.* **1998**, *80*, 1357–1360.

(42) Wales, D. J.; Scheraga, H. A. *Science* **1999**, *285*, 1368–1372.

(43) Wales, D. J. *Energy Landscapes*; Cambridge University Press: Cambridge, 2003.

(44) Sugita, Y.; Okamoto, Y. *Chem. Phys. Lett.* **1999**, *314*, 141–151.

(45) Lazaridis, T.; Karplus, M. *Proteins: Struct., Func., Gen.* **1999**, *35*, 133–152.

(46) Neria, E.; Fischer, S.; Karplus, M. *J. Chem. Phys.* **1996**, *105*, 1902–1921.

(47) MacKerell, A. D.; Bashford, D.; Bellott, M.; Dunbrack, R. L.; Evanseck, J. D.; Field, M. J.; Fischer, S.; Gao, J.; Guo, H.; Ha, S.; Joseph-McCarthy, D.; Kuchnir, L.; Kuczera, K.; Lau, F. T. K.; Mattos, C.; Michnick, S.; Ngo, T.; Nguyen, D. T.; Prodhom, B.; Reiher, W. E.; Roux, B.; Schlenkrich, M.; Smith, J. C.; Stote, R.; Straub, J.; Watanabe, M.; Wiorkiewicz-Kuczera, J.; Yin, D.; Karplus, M. *J. Phys. Chem. B* **1998**, *102*, 3586–3616.

(48) Mackerell, A. D.; Feig, M.; Brooks, C. L. *J. Comput. Chem.* **2004**, *25*, 1400–1415.

(49) MacKerell, A. D.; Feig, M.; Brooks, C. L. *J. Am. Chem. Soc.* **2004**, *126*, 698–699.

(50) Feig, M.; MacKerell, A. D.; Brooks, C. L. *J. Phys. Chem. B* **2003**, *107*, 2831–2836.

(51) Li, Z.; Scheraga, H. A. *Proc. Natl. Acad. Sci. USA* **1987**, *84*, 6611–6615.

(52) Mezey, P. G. *Potential Energy Hypersurfaces*; Elsevier: Amsterdam, 1987.

(53) Wales, D. J. *J. Chem. Soc., Faraday Trans.* **1992**, *88*, 653–657.

(54) Derreumaux, P. *J. Chem. Phys.* **1997**, *106*, 5260–5270.

(55) Derreumaux, P. *J. Chem. Phys.* **1997**, *107*, 1941–1947.

(56) Miller, M. A.; Wales, D. J. *J. Chem. Phys.* **1999**, *111*, 6610–6616.

(57) Mortenson, P. N.; Wales, D. J. *J. Chem. Phys.* **2001**, *114*, 6443–6454.

(58) Mortenson, P. N.; Evans, D. A.; Wales, D. J. *J. Chem. Phys.* **2002**, *117*, 1363–1376.

(59) Carr, J. M.; Wales, D. J. *J. Chem. Phys.* **2005**, *123*, 234901.

(60) Verma, A.; Schug, A.; Lee, K. H.; Wenzel, W. *J. Chem. Phys.* **2006**, *124*, 044515.

(61) Mortenson, P. N.; Wales, D. J. *J. Chem. Phys.* **2001**, *114*, 6443–6454.

(62) Feig, M.; Karanicolas, J.; Brooks, C. L. *J. Mol. Graph. Mod.* **2004**, *22*, 377–395.

(63) Swendsen, R. H.; Wang, J.-S. *Phys. Rev. Lett.* **1986**, *57*, 2607–2609.

(64) Ryckaert, J. P.; Ciccotti, G.; Berendsen, H. J. C. *J. Comp. Phys.* **1977**, *23*, 327–341.

(65) Andersen, H. C. *J. Comp. Phys.* **1983**, *52*, 24–34.

(66) Chocholoušová, J.; Feig, M. *J. Comput. Chem.* **2006**, *27*, 719–729.

(67) Kumar, S.; Bouzida, D.; Swendsen, R. H.; Kollman, P. A.; Rosenberg, J. M. *J. Comput. Chem.* **1992**, *13*, 1011–1021.

(68) Klimov, D. K.; Newfield, D.; Thirumalai, D. *Proc. Natl. Acad. Sci. USA* **2002**, *99*, 8019–8024.

(69) Pellarin, R.; Caflisch, A. *J. Mol. Biol.* **2006**, *360*, 882–892.

(70) Hutchinson, E. G.; Thornton, J. M. *Protein Sci.* **1994**, *3*, 2207–2216.

(71) Dang, L. X.; Pettitt, B. M. *J. Am. Chem. Soc.* **1987**, *109*, 5531–5532.

(72) Friedman, G. L. *Faraday Discuss. Chem. Soc.* **1988**, *85*, 1–11.

(73) Masunov, A.; Lazaridis, T. *J. Am. Chem. Soc.* **2003**, *125*, 1722–1730.

(74) Cecchini, M.; Rao, F.; Seeber, M.; Caflisch, A. *J. Chem. Phys.* **2004**, *121*, 10748.

(75) Paci, E.; Gsponer, J.; Salvatella, X.; Vendruscolo, M. *J. Mol. Biol.* **2004**, *340*, 555–569.

(76) Feig, M.; Onufriev, A.; Lee, M. S.; Im, W.; Case, D. A.; Brooks, C. L. *J. Comput. Chem.* **2004**, *25*, 265–284.

(77) Chen, J.; Im, W.; Brooks, C. L. *J. Am. Chem. Soc.* **2006**, *128*, 3728–3736.

(78) Gazit, E. *FASEB J.* **2002**, *16*, 77–83.

(79) Schaefer, M.; Bartels, C.; Leclerc, F.; Karplus, M. *J. Comput. Chem.* **2001**, *22*, 1857–1879.

(80) Press, W. H.; Teukolsky, S. A.; Vetterling, W. T.; Flannery, B. P. *Numerical Recipes in FORTRAN*, 2 ed.; Cambridge University Press: Cambridge, 1992.

(81) Lebedev, V. I.; Laikov, D. N. *Doklady Math.* **1999**, *59*, 477–481.

(82) Verlet, L. *Phys. Rev.* **1967**, *159*, 98–103.

(83) Verlet, L. *Phys. Rev.* **1967**, *165*, 201–214.

(84) Evans, D. J.; Holian, B. L. *J. Chem. Phys.* **1985**, *83*, 4069–4074.

(85) Steinbach, P. J.; Brooks, B. R. *J. Comput. Chem.* **1994**, *15*, 667–683.

(86) Bogusz, S.; Cheatham, T.; Brooks, B. *J. Chem. Phys.* **1998**, *108*, 7070–7084.

(87) Wales, D. J. *Mol. Phys.* **2002**, *100*, 3285–3306.

(88) Wales, D. J. *Int. Rev. Phys. Chem.* **2006**, *25*, 237–282.

CT700305W